Nitrogen-Doped Graphene and Its Iron-Based Composite As Efficient Electrocatalysts for Oxygen Reduction Reaction

Khaled Parvez,[†] Shubin Yang,[†] Yenny Hernandez,[†] Andreas Winter,[‡] Andrey Turchanin,[‡] Xinliang Feng,[†,*] and Klaus Müllen[†,*]

[†]Max Planck Institute for Polymer Research, Ackermannweg 10, D-55128 Mainz, Germany and [‡]Faculty of Physics, University of Bielefeld, Universitätsstraße 25, D-33615 Bielefeld, Germany

ABSTRACT The high cost of platinum-based electrocatalysts for the oxygen reduction reaction (ORR) has hindered the practical application of fuel cells. Thanks to its unique chemical and structural properties, nitrogen-doped graphene (NG) is among the most promising metal-free catalysts for replacing platinum. In this work, we have developed a cost-effective synthesis of NG by using cyanamide as a nitrogen source and graphene oxide as a precursor, which led to high and controllable nitrogen contents (4.0% to 12.0%) after pyrolysis. NG thermally treated at 900 °C shows a stable methanol crossover effect, high current density (6.67 mA cm^{-2}), and durability (~87% after 10 000 cycles) when catalyzing ORR in alkaline solution. Further, iron (Fe) nanoparticles could be incorporated into NG with the aid of Fe(III) chloride in the synthetic process. This allows one to examine the influence of non-noble metals on the electrocatalytic performance. Remarkably, we found that NG supported with 5 wt % Fe nanoparticles displayed an excellent methanol crossover effect and high current density (8.20 mA cm^{-2}) in an alkaline solution. Moreover, Fe-incorporated NG showed almost four-electron transfer processes and superior stability in both alkaline (~94%) and acidic (~85%) solutions, which outperformed the platinum and NG-based catalysts.

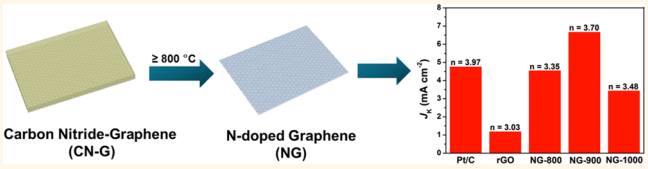

KEYWORDS: graphene oxide · nitrogen-doped graphene · iron coordination · oxygen reduction reaction · stability

The cathodic oxygen reduction reaction (ORR) plays a crucial role in electrochemical energy conversion in fuel cells.[1] Platinum-based materials have long been used as active catalysts for the ORR; however, these noble metal catalysts hinder widespread commercialization of fuel cells due to their high cost, sluggish electron transfer kinetics, and limited supply.[2−4] Moreover, during a long-term electrochemical process, Pt-based catalysts generally suffer from surface oxide formation, particle dissolution, and aggregation in alkaline electrolytes.[5,6] Therefore, numerous efforts have been devoted to finding a suitable substitute for Pt-based catalysts including nitrogen-doped carbon nanotubes,[7−9] mesoporous graphitic arrays,[10] and nonprecious transition metal catalysts (such as iron or cobalt coordinated to nitrogen-doped carbons).[11,12] The advantages of these alternative catalysts include low cost, excellent electrocatalytic activity, long durability, and an environmentally benign character. In general, the transition metal catalysts can be synthesized by pyrolyzing precursors containing nitrogen, Fe or Co salts, and macrocyclic compounds (such as Co(II) or Fe(II) phthalocyanine or methoxyphenyl porphyrin) adsorbed on carbon black (CB).[12−16] However, when the pyrolysis temperature is higher than 800 °C, gasification of CB occurs, especially in the presence of NH_3; this results in mass loss of carbon and consequently shortens the lifespan of these catalysts.[17,18] Although the nature of nitrogen atoms in nitrogen-doped carbon materials and the catalytically active sites in metal−nitrogen−carbon (M−N−C) remain controversial,[19,20] both quantum mechanical calculations[21] and experimental investigations[22] indicate that pyridinic and/or graphitic nitrogen moieties play an essential role in catalyzing the ORR.[23]

Graphene is a monolayer of carbon atoms arranged in a two-dimensional honeycomb

* Address correspondence to muellen@mpip-mainz.mpg.de, feng@mpip-mainz.mpg.de.

Received for review June 17, 2012 and accepted October 10, 2012.

Published online October 10, 2012
10.1021/nn302674k

network. It shows many intriguing properties such as high surface area,[24] excellent electrical conductivity,[25] and high thermal and chemical stability.[26] Recently, nitrogen-doped graphene (NG) has been shown to possess high electrocatalytic activity and long-term operational stability when catalyzing the ORR.[27] The high surface area of NG results in many active sites for coordination with Fe or Co, which may lead to enhanced electrochemical performance and hence improve catalysis of the ORR. However, there are only a handful of studies on the preparation of NG, including treating graphene in ammonia at high temperature,[28,29] using an ammonia plasma,[30] and growth of NG on Ni substrates by chemical vapor deposition (CVD).[27] All these processes require vacuum conditions and are difficult to scale up, which limits the practical use of NG. Therefore, an expeditious method to fabricate NG with controllable nitrogen moieties and high surface area is highly desirable.

Herein, we report the facile synthesis of NG by immobilizing graphitic carbon nitride (CN) on graphene sheets to form a carbon nitride–graphene composite (CN-G). The CN-G composite is then subjected to thermal treatment, leading to the decomposition of CN and thereby introducing nitrogen moieties into graphene. In this way, NG sheets with nitrogen content from 4.0% to 12.0% can be obtained by controlling the pyrolysis temperature. Furthermore, NG infused with iron nanoparticles (NG/Fe) can be synthesized by the addition of iron salts (*e.g.*, $FeCl_3$) into the CN-G. We show that NG containing 5.0 wt % Fe exhibits high electrocatalytic activity, low onset potential, excellent methanol crossover effect, and long-term stability in oxygen reduction reactions in both acid and alkaline solutions. These traits represent clear advantages over commercially available Pt-based electrodes (30 wt % Pt on Vulcan XC72).

RESULTS AND DISCUSSION

The synthesis of NG is illustrated in Figure 1. In the first step, graphene oxide (GO) was modified by a surfactant (sodium dodecylbenzenesulfonic acid, SDBS) to enhance the dispersion of GO in water. Afterward, cyanamide (4 mL) was added dropwise into the GO (1 mg/mL) solution (see Experimental Section for details). The mixture was then heated to 100 °C, with continuous stirring, to remove water. Subsequently, the resultant solid powder was annealed at 550 °C under an argon flow for 4 h to trigger the thermal condensation of cyanamide, providing polymeric CN.[31] Further heat treatment of the CN-G at 800, 900, and 1000 °C gave rise to CN decomposition and thereby generated NG. For simplicity, the samples are denoted as NG-800, NG-900, and NG-1000, respectively.

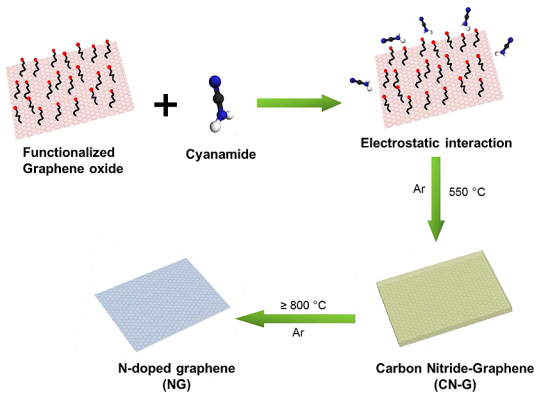

Figure 1. Preparation of NG for ORR.

The morphology and structure of CN-G were first investigated by transmission electron microscopy (TEM) and scanning electron microscopy (SEM). CN without incorporation of graphene sheets shows a typical slate-like morphology,[32] while CN-G becomes crumpled (Figure S1) due to the adsorbed cyanamide on graphene, which undergoes polymerization under thermal treatment. As indicated in Figure 2a, graphene sheets were not distinctively visible in CN-G due to the thick layer of CN adsorbed on the graphene surface. The XRD patterns of CN, which stacks like graphite with a tri-*s*-triazine unit, feature two diffraction peaks at around 27.2° and 13.1°.[31] After the introduction of graphene, the unchanged X-ray diffraction (XRD) pattern suggests that graphene sheets are homogeneously distributed in CN without disrupting their solid-state packing (Figure 2b).

Thermogravimetric analysis (TGA) of CN-G containing 5.0 wt % of graphene reveals that weight loss starts at around 600 °C (Figure S2), which can be assigned to the decomposition of CN. After treatment at 800 °C, a total ~95% weight loss of the composite suggests that only graphene remains. TEM images (Figures 2c and S3) of the NG-800, NG-900, and NG-1000 demonstrate transparent graphene sheets without the presence of any residual CN. A Brunauer–Emmett–Teller (BET) surface area of 508 $m^2\ g^{-1}$ for NG-900 (Figure S4) is obtained, which is higher than that of NG produced by other methods.[33,34] In addition, a narrow pore-size distribution centered at about 3.1 nm and a total pore volume of 3.674 $cm^3\ g^{-1}$ can be derived from the adsorption branch of the isotherms based on the Barrett–Joyner–Halenda (BJH) model.

To probe the chemical composition and content of nitrogen in NG, X-ray photoelectron spectroscopic (XPS) measurements were carried out on NG-800, NG-900, and NG-1000 (Figures 2d and S5). As shown in Figure 2d, the survey spectra of NG samples reveal the presence of C, O, and N and a nitrogen content of 12.0%, 5.0%, and 4.0% in NG-800, NG-900, and

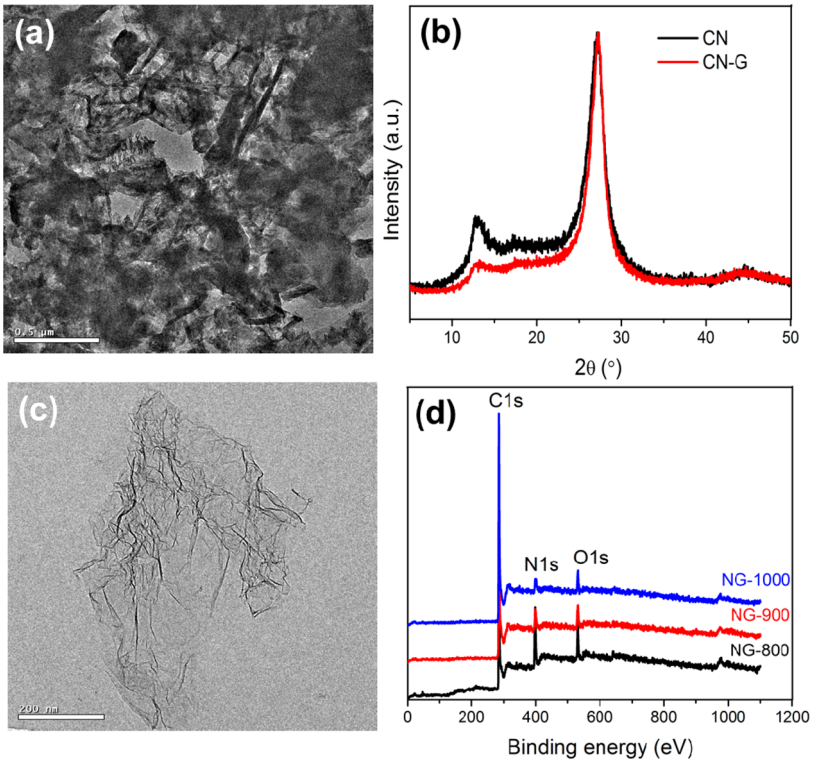

Figure 2. (a) TEM image and (b) XRD pattern of CN and CN-G composite, (c) TEM image of CN-G composite after pyrolyzing at 900 °C (*i.e.*, NG-900), and (d) XPS survey of NG samples.

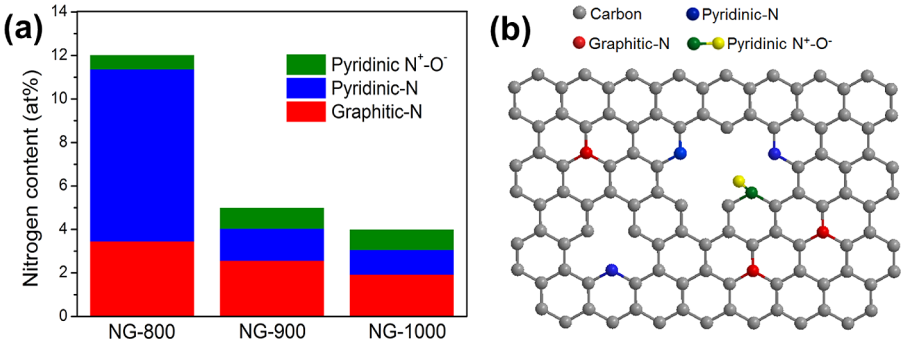

Figure 3. (a) The content of three types of nitrogen in NG. (b) Schematic representation of NG.

NG-1000, respectively. This is consistent with the values determined by elemental analysis (Figure S5). Furthermore, the absence of an S 2p peak at 165.0 eV (Figure S5e) indicates that the surfactant (SDBS) was completely decomposed upon pyrolysis. The C 1s peaks for the NG samples (Figure S6a) center at approximately 284.6 eV and are slightly asymmetric. This is a common effect for nitrogen-doped carbon materials.[35] The width of the C 1s peaks becomes smaller as the pyrolysis temperature increases from 800 to 1000 °C, suggesting enhanced graphitization at higher temperature. This result is further supported by the Raman spectrum (Figure S7); the G band becomes sharper and the intensity ratio of the G to the D band (I_G/I_D) increases.[36] Analysis of N 1s spectra reveals the presence of pyridinic and graphitic nitrogen, corresponding to binding energies of 398.4 and 401.0 eV, respectively (Figure S6).[23] In addition, the reaction between oxygen-containing groups in GO and nitrogen species during the synthesis results in the formation of pyridinic N^+-O^- at 402.0–404.0 eV.[37] In NG-800, pyridinic-N is more prevalent than graphitic-N, with contents of 7.92% and 3.45%, respectively (Figure 3a). Upon raising the pyrolysis temperature to 900 and 1000 °C, the overall nitrogen content decreases dramatically. Interestingly, the pyridinic-N content largely drops to 1.47% at 900 °C and 1.14% at 1000 °C, whereas the graphitic-N slowly decreases. However, the content of graphitic-N is higher than that of pyridinic-N at 900 and 1000 °C. Furthermore, the ratio of graphitic-N to pyridinic-N content in NG-800, NG-900, and NG-1000 shows significant differences (*i.e.*, 0.44, 1.73, and 1.66, respectively). A slight

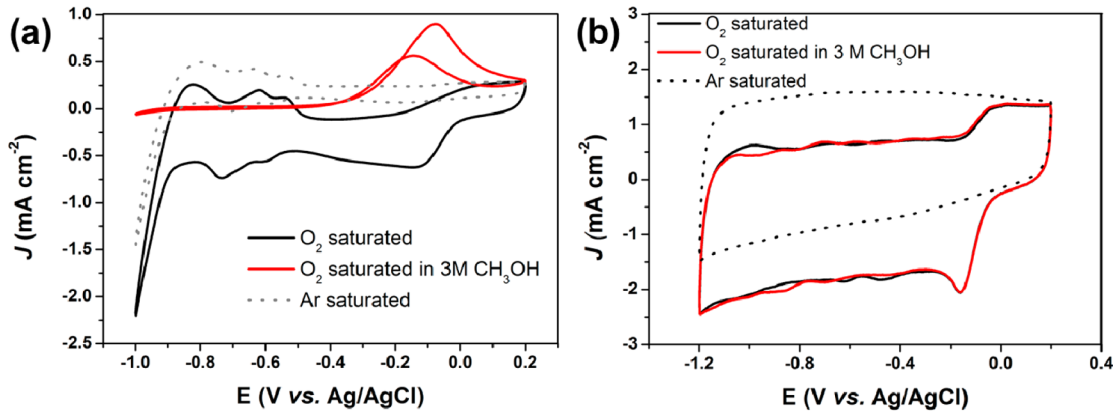

Figure 4. Cyclic voltammograms of (a) NG-900 and (b) Pt/C at a scan rate of 100 mV cm^{-1} in O_2- or Ar-saturated 0.1 M KOH solutions as well as O_2-saturated 0.1 M KOH solution with 3 M CH_3OH.

increase in pyridinic N^+-O^- is observed from NG-800 to NG-900, but remains unchanged in NG-1000. This type of nitrogen species does not significantly contribute to the ORR performance and is unstable under fuel cell operating conditions.[38] Therefore, such different amounts of nitrogen-bonding configurations in NG samples are expected to play a crucial role in the ORR electrocatalytic performances.[39] The XRD of NG samples in Figure S8 shows a pronounced broad peak at 26.1°, attributable to the π-stacking of graphene sheets.[27] The absence of a diffraction peak at 13.1° also suggests that CN is successfully removed upon pyrolysis. The N-doping may lead to an increased interlayer spacing in NG,[27] and as the nitrogen content decreases from NG-800 to NG-1000, the diffraction peaks become sharper.

The electrocatalytic activity of NG for the ORR was first examined—in a 0.1 M KOH solution saturated with argon or oxygen—by cyclic voltammetry (CV) at a scan rate of 100 mV s^{-1}. As shown in Figure 4a, featureless voltammetric currents within the potential range of −1.2 to +0.2 V were observed for NG-900 in the argon-saturated solution (dotted curve). In contrast, when the electrolyte was saturated with O_2, a well-defined cathodic peak centered at −0.16 V was detected, suggesting pronounced electrocatalytic activity of NG-900. A possible crossover effect in NG-900 and Pt/C against the electrooxidation of methanol in O_2-saturated 0.1 M KOH in the presence of methanol (3.0 M) was also detected. The Pt/C shows a pair of peaks at −0.15 and −0.08 V, corresponding to methanol oxidation, whereas the cathodic peak for the ORR disappears (Figure 4b). In contrast, no noticeable change was seen in the oxygen reduction current on NG-900 under the same experimental conditions (Figure 4a), suggesting high selectivity and good stability of NG-900 for the ORR with respect to Pt/C.

To further evaluate the electrocatalytic activity of NG, both rotating ring disk electrodes (RRDE) and rotating disk electrodes (RDE) were employed. Figure 5a shows the steady-state voltammograms for different NG samples loaded on a glassy carbon electrode in O_2-saturated 0.1 M KOH. The corresponding ring current (I_R) for the oxidation of hydrogen peroxide ions (HO_2^-) was measured with a Pt ring electrode with a potential of 0.50 V. The electron transfer number per oxygen molecule involved in the ORR of the NG-800, NG-900, and NG-1000 electrodes was calculated to be 3.35, 3.70, and 3.48, respectively. The calculation used eq 1[7] and a potential of −0.4 V.

$$n = 4I_D/(I_D + I_R/N) \quad (1)$$

where $N = 0.36$ is the collection efficiency, I_D is the disk current, and I_R is the ring current. The lower ring current of NG-900 compared to NG-800 and NG-1000 suggests that a lower amount of HO_2^- reached the ring electrode under increasing negative potentials. The onset potential of NG-900 was determined to be −0.03 V, which is close to that identified from CV measurements (−0.04 V, Figure 5a). Different from a Pt/C electrode, the NG-900 electrode showed an enhanced steady-state diffusion current over a large potential range.

The current density (J_K) of the NG samples was analyzed by RDE and calculated on the basis of the Koutecky−Levich equations (eqs 2−4).[10]

$$\frac{1}{J} = \frac{1}{J_L} + \frac{1}{J_K} = \frac{1}{B\omega^{1/2}} + \frac{1}{J_K} \quad (2)$$

$$B = 0.62nFC_0(D_0)^{2/3}\nu^{-1/6} \quad (3)$$

$$J_K = nFkC_0 \quad (4)$$

where J is the measured current density, J_K and J_L are the kinetic- and diffusion-limiting current densities, ω is the angular velocity of the disk ($\omega = 2\pi N$, N is the linear rotation speed), n is the overall number of electrons transferred in the oxygen reduction, F is the Faraday constant (96 485 C mol^{-1}), C_0 is the bulk concentration of O_2, ν is the kinematic viscosity of

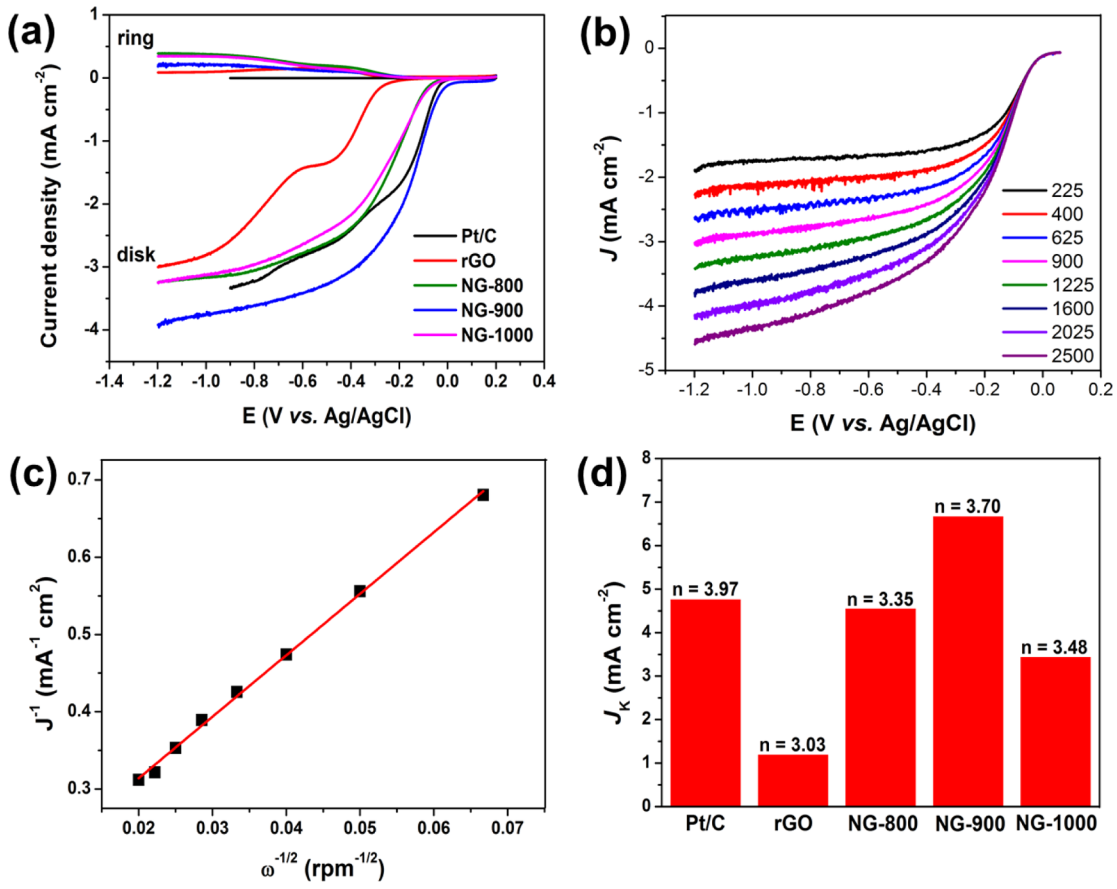

Figure 5. (a) RRDE voltammetric response for the ORR in O_2-saturated 0.1 M KOH at a scan rate of 10 mV s^{-1}. The electrode rotation rate was 1600 rpm, and the Pt ring electrode was polarized at 0.5 V; (b) RDE voltammograms recorded for NG-900 supported on a GC electrode in an O_2-saturated 0.1 M KOH solution at a scan rate of 10 mV s^{-1} and different rotation rates; (c) Koutecky–Levich plot of J^{-1} *vs* $\omega^{-1/2}$ at −0.4 V obtained from (b); and (d) electrochemical activity given as the kinetic-limiting current density (J_K) at −0.4 V for Pt/C, rGO, and all three NG electrodes.

the electrolyte, and k is the electron transfer rate constant. The Koutckey–Levich plot of J^{-1} *vs* $\omega^{-1/2}$ at a potential of −0.40 V on the NG-900 electrode exhibited good linearity (Figure 5c). As shown in Figure 5d, the calculated J_K value of 6.67 mA cm^{-2} at −0.40 V is much higher than that of Pt/C (4.76 mA cm^{-2} at −0.40 V) and is comparable or even higher than previous reports on nitrogen-doped graphene, CNTs, and other types of carbon materials.[27,29,40,41] In association with the XPS and electrochemical results described for NG-800, NG-900, and NG-1000, the content of pyridinic-N among the different nitrogen species does not play a significant role in the performance of the ORR. In contrast, the electrochemical performance is dependent on the content of graphitic-N, for which a higher ratio of graphitic-N over pyridinic-N in NG-900 than NG-800 and NG-1000 might be responsible for the high catalytic performance.[10]

It has been reported that the pyridinic nitrogen enriched carbon material can be favorable for the fabrication of Fe–N–C-based catalysts.[42] Given that the present synthetic approach offers a high content of pyridinic-N sites in the CN-G composite, one can expect that the introduction of Fe salts to CN-G will lead to an incorporation of Fe nanoparticles into NG and provide efficient coordination between Fe and pyridinic-N. Toward this end, NG decorated with Fe nanoparticles was prepared by mixing $FeCl_3$ with the precursors GO and cyanamide, followed by subsequent thermal treatment at 900 °C (Figure S9). The detailed procedure can be found in the Experimental Section. NG samples with different Fe content were prepared in this work and are denoted as NG/Fe_x (where x = 2.0, 5.0, 10.0, and 15.0 wt %).

Figure 6a shows the XRD pattern of NG/$Fe_{5.0}$. The diffraction peak at 42.8° is characteristic for Fe(110). In addition, HRTEM images display the presence of small (2–4 nm) crystalline Fe nanoparticles on NG. They also show a lattice d-spacing of ~0.23 nm, which is slightly higher than the standard value of 0.203 nm (JCPDS database) (Figure 6b and c). The larger d-spacing might be attributed to Fe nanoparticles incorporated into the nitrogen lattice, which enlarges the lattice constant.[43] The presence of N and Fe in the composite can be further validated by the corresponding energy dispersive X-ray (EDX)

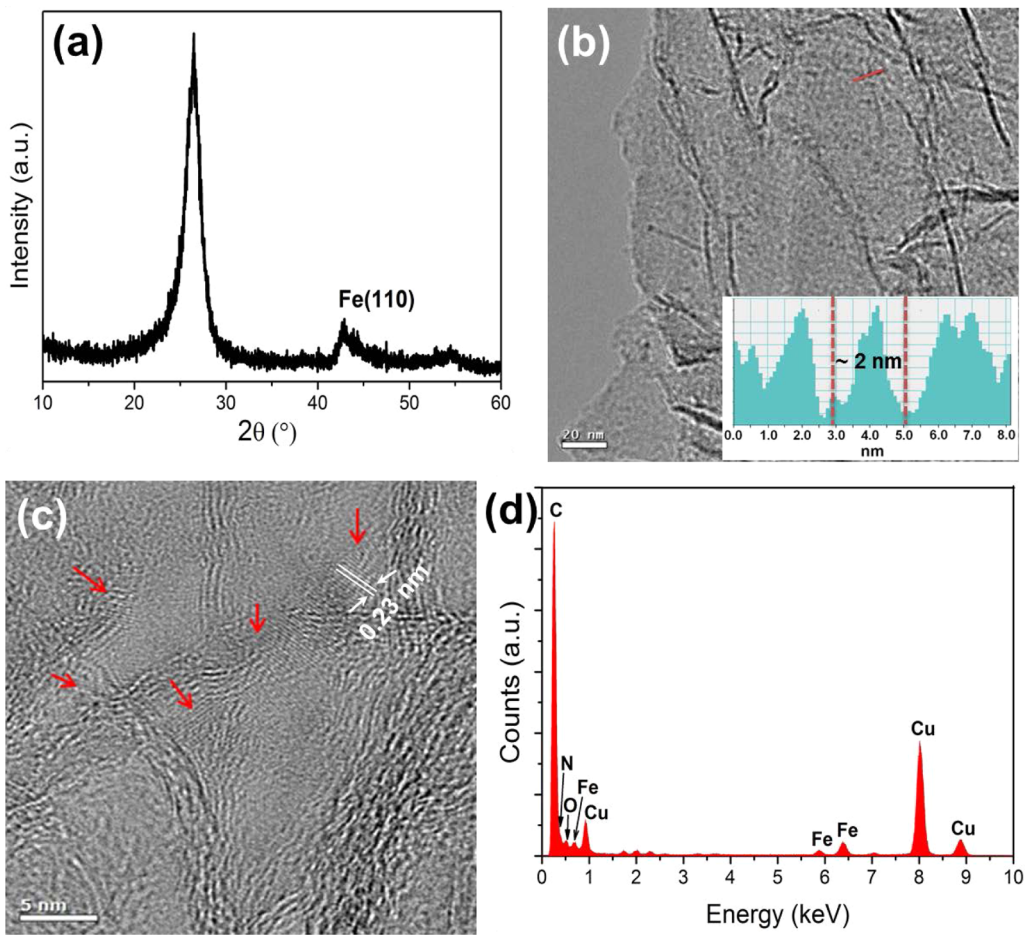

Figure 6. (a) XRD pattern of NG/$Fe_{5.0}$ composite, (b) TEM image of NG/$Fe_{5.0}$ with particle size distribution of the area indicated by small red line (inset), (c) HRTEM images of NG/$Fe_{5.0}$ showing the presence of crystalline Fe nanoparticles (indicated by arrows) on NG; and (d) corresponding EDX spectra of NG/$Fe_{5.0}$.

analysis (Figure 6d). Increasing the Fe content to 15.0 wt % (*i.e.*, NG/$Fe_{15.0}$) results in the agglomeration of ~50 nm Fe nanoparticles. In contrast, no large nanoparticles were visible in NG/$Fe_{5.0}$ (Figure S10a, b). The XPS survey spectrum of NG/$Fe_{5.0}$ shows the presence of Fe 2p and Fe 3p, in addition to N 1s, C 1s, and O 1s peaks (Figure S11). Unfortunately, the Fe 3p peak (~52−56 eV) is too weak to determine the valence state of Fe.

The catalytic properties of NG/Fe_x samples were first assessed with cyclic voltammetry in a 0.1 M KOH solution. The NG/$Fe_{5.0}$ shows a featureless voltammetric current within the potential range of −1.2 to +0.2 V in an Ar-saturated alkaline solution (Figure S12). Saturating the electrolyte with O_2 results in a well-defined cathodic peak at ~0.20 V. Similar to NG-900, NG/$Fe_{5.0}$ did not show any change in the oxygen reduction current in an O_2-saturated alkaline solution in the presence of 3.0 M methanol, making the catalyst very stable against crossover effects. However, two additional peaks were observed at −0.61 and −0.93 V, which are associated with the redox reaction of the iron nanoparticles.[7] Figure 7a shows the RRDE polarization curves of NG/Fe_x composites supported on a glassy carbon electrode in O_2-saturated 0.1 M KOH. The electron transfer number for NG/Fe_x samples, at the potential of −0.4 V, was calculated to be 3.79, 3.91, 3.80, and 3.79 for the NG/$Fe_{2.0}$, NG/$Fe_{5.0}$, NG/$Fe_{10.0}$, and NG/$Fe_{15.0}$, respectively. All samples of NG loaded with Fe nanoparticles greatly enhanced the electrochemical performance, leading to four electron transfer processes in the ORR. Although the onset potential for the ORR at the NG/$Fe_{5.0}$ electrode was similar (*i.e.*, −0.04 V) to that of Pt/C, the reduction current was significantly higher (Figure S12). As shown in Figure 7b, the calculated current density (J_K) value of NG/$Fe_{2.0}$, NG/$Fe_{5.0}$, NG/$Fe_{10.0}$, and NG/$Fe_{15.0}$ is 3.57, 8.20, 7.69, and 5.26 mA cm^{-2}, respectively. This result suggests that increasing the Fe content leads to an increase in the concentration of active catalytic sites until all pyridinic-N is coordinated (at 5.0 wt %).[44] Increasing the Fe content from 5.0 wt % to 10.0 and 15.0 wt % produces uncoordinated metal particles (Figure S10), which do not provide additional catalytic sites.[45] Therefore, no enhancement of the current density or electron transfer number was observed for NG/$Fe_{10.0}$ and NG/$Fe_{15.0}$. It is remarkable to note that NG/$Fe_{5.0}$ has a current density almost 2 times higher than Pt/C

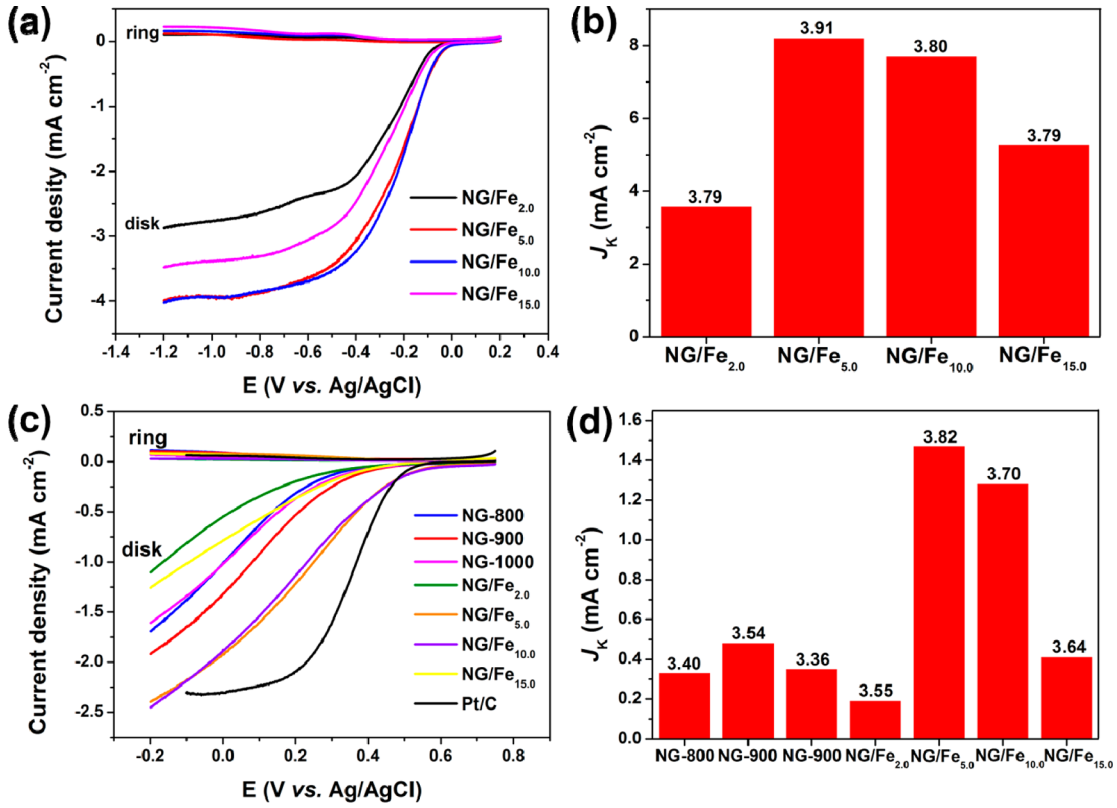

Figure 7. (a) RRDE polarization curves of NG/Fe$_x$ samples in O$_2$-saturated 0.1 M KOH at a scan rate of 10 mV s^{-1} and 1600 rpm electrode rotation rate; (b) electrochemical activity given as the kinetic-limiting current density (J_K) of the NG/Fe$_x$ series supported on GC electrodes at −0.4 V; (c) RRDE curves of NG and NG/Fe$_x$ series in O$_2$-saturated 0.5 M H$_2$SO$_4$ at a scan rate of 10 mV s^{-1} and 1600 rpm electrode rotation rate; and (d) electrochemical activity given as the kinetic-limiting current density (J_K) of NG and NG/Fe$_x$ series supported on GC electrodes at 0.2 V. The electron transfer number (n) in (b) and (d) was obtained from RRDE.

(4.76 mA cm^{-2}). This suggests that incorporating Fe nanoparticles into NG provides a synergistic coupling between Fe and NG that results in an outstanding electrocatalytic performance compared to Pt/C and NG-900.

Another set of NG/Fe$_x$ samples were prepared by treatment at 800 and 1000 °C. Figure S14 shows the summarized results of electron transfer number and J_K values obtained from both RRDE and RDE. The catalytic performance of NG/Fe$_{5.0}$ (at 800 °C) is lower than that of the samples prepared at 900 °C (Figure S13a). Surprisingly, NG/Fe$_{5.0}$ prepared at 1000 °C (Figure S14b) showed a higher electron transfer number and J_K than samples prepared at 800 °C and slightly lower values than NG/Fe$_{5.0}$ prepared at 900 °C. This result suggests that the oxygen reduction reaction rate increases with heat-treatment temperature of the catalysts, reaching a plateau at <1000 °C.[46,47] Thus, it can be concluded that the higher content of pyridinic-N alone (by lower temperature treatment) does not necessarily result in high catalytic performance. In addition, the temperature for catalyst preparation plays an important role in the synergistic coupling between Fe and nitrogen components in the composites.

Furthermore, NG/Fe$_x$ composites also showed high ORR activity in acidic solution. Both RRDE and RDE measurements were carried out in 0.5 M H$_2$SO$_4$ solution (Figure 7c and d). All the NG samples containing Fe again showed higher electron transfer numbers compared to NG samples at the potential of 0.2 V vs Ag/AgCl. At 1600 rpm, the NG/Fe$_{5.0}$ showed a maximum J_K of about 1.47 mAcm^{-2} with almost four-electron transfer (n = 3.82) processes and the lowest onset potential (0.47 V *vs* Ag/AgCl) of all tested electrodes. The catalytic activity order of the NG/Fe$_x$ catalysts in acidic medium was the same as that in alkaline medium, but they showed much higher current density in the alkaline solution.

To examine the influence of any uncoordinated Fe nanoparticles (*i.e.*, Fe residues) in the NG/Fe$_x$ composites on the electrocatalytic performance, NG/Fe$_{5.0}$ was first treated in 2 M H$_2$SO$_4$ at 80 °C for 3 h and again subjected to ORR measurements in alkaline and acidic solutions. Remarkably, the acid-treated NG/Fe$_{5.0}$ showed almost the same ORR catalytic activity and a similar onset potential, electron transfer number, and current density in both acidic and alkaline media (Figure 8). This result shows that Fe residues do not significantly contribute to the ORR performance.

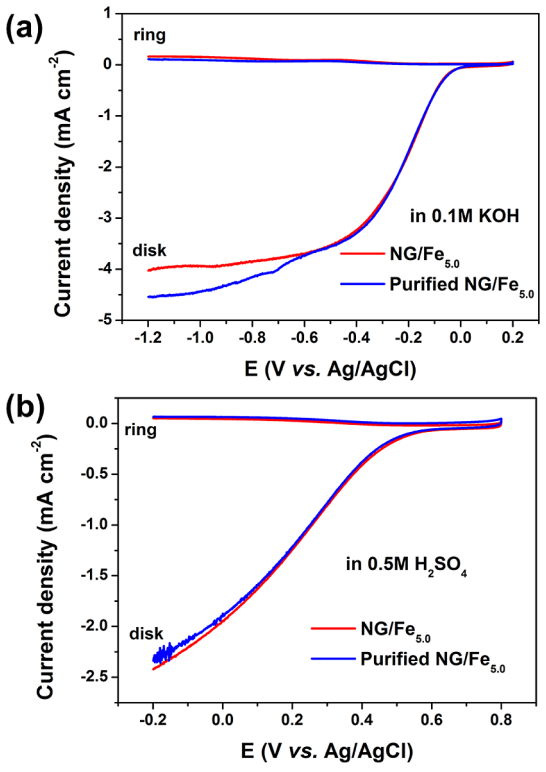

Figure 8. RRDE polarization curves of purified and unpurified NG/$Fe_{5.0}$ in O_2-saturated (a) 0.1 M KOH and (b) 0.5 M H_2SO_4 solution at a rotation rate of 1600 rpm.

The stability of NG-900, NG/$Fe_{5.0}$, and Pt/C electrodes toward the ORR was first examined by continuous potential cycling between +0.2 and −1.2 V in O_2-saturated 0.1 M KOH for 10 000 cycles (Figure S13). As indicated in Figure S15a, the deterioration of the Pt/C electrode resulted in a ~58% drop in current density. In contrast, NG-900 and NG/$Fe_{5.0}$ electrodes showed only a slight decay of current density, ~13% and ~6% at −0.15 V, respectively (Figure S15b and c). The voltammetric response of the two electrodes also remained unchanged after the continuous potential cycles. In addition, the NG/$Fe_{5.0}$ showed only ~15% decay in the current density (at 0.38 V) in acidic medium after 10 000 cycles (Figure S12d). These results show that NG/$Fe_{5.0}$ exhibited superior durability over Pt/C-based catalysts.

CONCLUSION

In summary, we report a facile and scalable method to prepare NG to catalyze the ORR in a fuel cell. The prominent features of synthesized NG include high nitrogen content, high surface area, high electrocatalytic activity, and superior durability. The incorporation of Fe nanoparticles into the NG results in significantly enhanced performance of graphene-based catalysts. These NG/F_x catalysts feature the almost four-electron transfer processes, high current density, and superb stability. They also outperform Pt/C toward ORR in both acidic and alkaline media. In addition to their promising application as fuel cell catalysts, we anticipate that NG with and without metal nanoparticles will provide broad applications in the field of lithium ion batteries, sensors, field-effect transistors, and supercapacitors.

EXPERIMENTAL SECTION

Synthesis of GO, NG, and NG/Fe_x Composites. Graphite oxide was prepared from natural graphite by a modified Hummers method.[48] Graphene−carbon nitride (G-CN) composites were prepared by electrostatic interaction between anionic surfactant modified graphene oxide and cyanamide precursor for synthesizing carbon nitride. In a typical synthesis, 0.1 g of the surfactant sodium dodecylbenzenesulfonic acid was mixed with 100 mL of GO dispersion (1 mg/mL) in water and sonicated for 30 min. Then, 4 mL of cyanamide solution (50 wt % in water) was added dropwise. The mixture was then stirred continuously and heated at 100 °C to remove water. The resulting solid was calcined in two different steps. In the first step, the solid products were heated to 550 °C at a rate of 2 °C/min and tempered at this temperature for another 4 h to form CN.[31] To prepare NG, the resulting CN-G composites were further heated to 800, 900, and 1000 °C. All the sample annealing and cooling processes were carried out under argon flow. For comparison, undoped and reduced GO (rGO) was also prepared by pyrolyzing pure GO under the same annealing processes.

Composites of NG with iron nanoparticles were synthesized by adding the desired amount (*i.e.*, 2, 5, 10, and 15 mg) of $FeCl_3$ to 100 mg of GO solution (1 mg/mL) and sonicating the mixture for 1 h. The content of Fe (*i.e.*, 2.0, 5.0, 10.0, and 15.0 wt %) in the composites was calculated with respect to the total mass of GO into the solution. Then 4 mL of cyanamide solution was added dropwise. The reaction mixture was then heated at 100 °C with continuous stirring to remove water. The resulting solid was then calcined at 550 °C for 4 h to form CN and then pyrolyzed separately at 800, 900, and 1000 °C for 1 h to decompose the CN. All the annealing processes were carried out under an argon atmosphere.

Characterization. The morphology and microstructures of the samples were investigated by HRTEM (Philips Tecnai F20), TGA (Mettler TG 50), and XRD (Bruker D4 X-ray scattering system with Ni-filtered Cu Kα radiation). Raman spectra were recorded with a Bruker RFS 100/S spectrometer. Nitrogen sorption isotherms and BET surface areas were measured at 77 K with a Micrometrics Tristar 3000 analyzer (USA). The chemical composition was analyzed by XPS with an Omicron Multiprobe spectrometer using Al Kα radiation. For these measurements CN-G composites were ultrasonicated in ethanol and then cast and dried at ambient conditions on Au substrates (30 nm Au films thermally evaporated on Cr-primed Si wafers, Georg-Albert PVD-Coatings). XPS binding energies were referenced to the Au $4f_{7/2}$ peak (84.0 eV). Elemental chemical ratios in CN-G composites were calculated from areas of the XP peaks. The calculations assumed a homogeneous distribution of elements in the samples and normalized the peak areas with Scofield sensitivity factors and electron attenuation lengths evaluated from the Laibinis expression. For the analysis of N1s spectra a Shirley background subtraction procedure was employed and symmetric Voigt functions (90% of Gaussian character) were used for fitting. All fits were self-consistent.

Electrocatalytic Activity Evaluation. The ORR activity and four-electron selectivity of the nitrogen-doped graphene samples were evaluated using a rotating disk electrode and a rotating ring disk electrode, respectively. RDE/RRDE measurements were performed using a CHI Electrochemical Station (model 760D) in

a conventional three-electrode electrochemical cell. Platinum wire and an Ag/AgCl, KCl (3 M) electrode were used as the counter and reference electrode, respectively. The preparation of a glassy carbon working electrode (5 mm in diameter) is as follows: prior to use the working electrode was polished mechanically with a 0.05 μm alumina slurry to obtain a mirror-like surface, then washed with Mill-Q water and acetone, and allowed to dry. One milligram of the prepared NG sample was dissolved in a 1 mL solvent mixture of Nafion (5 wt %) and water (v/v ratio = 1:9) using sonication. For comparison, a commercially available catalyst of 30 wt % Pt supported on carbon black (fuel cell grade) was used, and a 1 mg/mL Pt/C suspension was prepared according to the same procedure described above. The electrodes were allowed to dry at room temperature before the measurement. This leads to a catalyst (NG samples or Pt/C) loading of 50.91 μg cm^{-2}.

The RRDE experiments were carried out in an O_2-saturated 0.1 M KOH solution. The potential was varied from +0.2 to −1.2 V at a potential sweep of 10 mV s^{-1}; the ring potential was set to 0.5 V. First, the potential range was cyclically scanned between −1.2 and +0.2 V at a scan rate of 100 mV s^{-1} at ambient temperature after purging with O_2 or Ar gas for 15 min. Then the RRDE experiments were performed. RRDE experiments in acidic conditions were performed in an O_2-saturated 0.5 M H_2SO_4 solution within the potential range of +0.8 to −0.2 V at a potential sweep of 10 mV s^{-1} and a ring potential of 1.0 V.

Conflict of Interest: The authors declare no competing financial interest.

Acknowledgment. This work was financially supported by the Max Planck Society through the program ENERCHEM, DFG Priority Program SPP 1459, BMBF LiBZ Project, BMBF Graphenoid Project, ESF Project GOSPEL (ref no. 09-EuroGRAPHENE-FP-001), EU Project GENIUS, and ERC grant on NANOGRAPH.

Supporting Information Available: SEM, TGA of CN and CN-G samples; HRTEM, BET, XPS of C1s, N1s, and S 2p spectra, Raman characterizations of NG; synthetic scheme, TEM, XPS spectra, and electrochemical characterizations of NG/Fe_x samples. This material is available free of charge *via* the Internet at http://pubs.acs.org.

REFERENCES AND NOTES

1. Steele, B. C. H.; Heinzel, A. Materials for Fuel-Cell Technologies. *Nature* **2001**, *414*, 345–352.
2. Shao, Y. Y.; Liu, J.; Wang, Y.; Lin, Y. H. Novel Catalyst Support Materials for PEM Fuel Cells: Current Status and Future Prospects. *J. Mater. Chem.* **2009**, *19*, 46–59.
3. Chen, W.; Chen, S. W. Oxygen Electroreduction Catalyzed by Gold Nanoclusters: Strong Core Size Effects. *Angew. Chem., Int. Ed.* **2009**, *48*, 4386–4389.
4. Chen, W.; Kim, J. M.; Sun, S. H.; Chen, S. W. Electrocatalytic Reduction of Oxygen by FePt Alloy Nanoparticles. *J. Phys. Chem. C* **2008**, *112*, 3891–3898.
5. Gewirth, A. A.; Thorum, M. S. Electroreduction of Dioxygen for Fuel-Cell Applications: Materials and Challenges. *Inorg. Chem.* **2010**, *49*, 3557–3566.
6. Jin, W.; Du, H.; Zheng, S. L.; Xu, H. B.; Zhang, Y. Comparison of the Oxygen Reduction Reaction between NaOH and KOH Solutions on a Pt Electrode: The Electrolyte-Dependent Effect. *J. Phys. Chem. B* **2010**, *114*, 6542–6548.
7. Gong, K. P.; Du, F.; Xia, Z. H.; Durstock, M.; Dai, L. M. Nitrogen-Doped Carbon Nanootube Arrays with High Electrocatalytic Activity for Oxygen Reduction Reaction. *Science* **2009**, *323*, 760–764.
8. Yu, D.; Zhang, Q.; Dai, L. Highly Efficient Metal-Free Growth of Nitrogen-Doped Single-Walled Carbon Nanotubes on Plasma-Etched Substrates for Oxygen Reduction. *J. Am. Chem. Soc.* **2010**, *132*, 15127–15129.
9. Feng, L.; Yan, Y.; Chen, Y.; Wang, L. Nitrogen-Doped Carbon Nanotubes as Efficient and Durable Metal-free Cathodic Catalysts for Oxygen Reduction in Microbial Fuel Cells. *Energy Environ. Sci* **2011**, *4*, 1892–1899.
10. Liu, R.; Wu, D. Q.; Feng, X.; Müllen, K. Nitrogen-Doped Ordered Mesoporous Graphitic Arrays with High Electrocatalytic Activity for Oxygen Reduction. *Angew. Chem Int. Ed.* **2010**, *49*, 2565–2569.
11. Lefèvre, M.; Proitetti, E.; Jaouen, F.; Dodelet, J. P. Iron-Based Catalysts with Improved Oxygen Reduction Activity in Polymer Electrolyte Fuel Cells. *Science* **2009**, *324*, 71–74.
12. Wu, G.; More, K. L.; Johnston, C. M.; Zelenay, P. High-Performance Electrocatalysts for Oxygen Reduction Derived from Polyaniline, Iron, and Cobalt. *Science* **2011**, *332*, 443–447.
13. Jasinski, R. A New Fuel Cell Cathode Catalyst. *Nature* **1964**, *201*, 1212–1213.
14. Gupta, S.; Tyrk, D.; Bae, I.; Aldred, W.; Yeager, E. Heat-Treated Polyacrylonitrile-Based Catalysts for Oxygen Electroreduction. *J. Appl. Electrochem.* **1989**, *19*, 19–27.
15. Schulenburg, H.; Stankov, S.; Schünemann, V.; Tributsch, H. Catalysts for Oxygen Reduction From Heat-Treated Iron (III) tetramethoxyphenylporphyrin chloride: Structure and Stability of Active Sites. *J. Phys. Chem. B* **2003**, *107*, 9034–9041.
16. Li, W.; Yu, A.; Higgins, D. C.; Llanos, B. G.; Chem, Z. Biologcally Inspired Highly Durable Iron Phthalocyanine Catalysts for Oxygen Reduction Reaction in Polymer Electrolyte Membrane Fuel Cells. *J. Am. Chem. Soc.* **2010**, *132*, 17056–17058.
17. Jaouen, F.; Lafèvre, M.; Dodelet, J. P.; Cai, M. Heat-Treated Fe/N/C Catalysts for O_2 Electroreduction: Are Active Sites Hosted in Micropores? *J. Phys. Chem. B* **2006**, *110*, 5553–5558.
18. Lafèvre, M.; Dodelet, J. P. Fe-Based Electrocatalysts Made with Microporous Pristine Carbon Black Support for the Reduction of Oxygen in PEM Fuel Cells. *Elecrochim. Acta* **2008**, *53*, 8269–8276.
19. Shao, Y. Y.; Sui, J. H.; Yin, G. P.; Gao, Y. Z. Nitrogen-Doped Carbon Nanostructures and Their Composites as Catalytic Materials for Proton Exchange Membrane Fuel Cells. *Appl. Catal., B* **2008**, *79*, 89–99.
20. Thorum, M. S.; Hankett, J. M.; Gewirth, A. A. Poisoning the Oxygen Reduction Reaction on Carbon-Supported Fe and Cu Electrocatalysts: Evidence for Metal-Centered Activity. *J. Phys. Chem. Lett.* **2011**, *2*, 295–298.
21. Ikeda, T.; Boero, M.; Haung, S. F.; Terakura, K.; Oshima, M.; Ozaki, J. Carbon Alloy Catalysts: Active Sites for Oxygen Reduction Reaction. *J. Phys. Chem. C* **2008**, *112*, 14706–14709.
22. Liu, G.; Li, X. G.; Ganesan, P.; Popov, B. N. Studies of Oxygen Reduction Reaction Active Sites and Stability of Nitrogen-Modified Carbon Composites for PEM Fuel Cells. *Electrochim. Acta* **2010**, *55*, 2853–2858.
23. Yang, S.; Feng, X.; Wang, X.; Müllen, K. Graphene-Based Carbon Nitride Nanosheets as Efficient Metal-Free Electrocatalysts for Oxygen Reduction Reactions. *Angew. Chem., Int. Ed.* **2011**, *50*, 5339–5343.
24. Stoller, M. D.; Park, S. J.; Zhu, Y. W.; An, J. H.; Rouff, R. S. Graphene-Based Ultracapacitors. *Nano Lett.* **2008**, *8*, 3498–3502.
25. Yang, S.; Feng, X.; Ivanovici, S.; Müllen, K. Fabrication of Graphene-Encapsulated Oxide Nanoparticles: Towards High-Performance Anode Materials for Lithium Storage. *Angew. Chem., Int. Ed.* **2010**, *49*, 8408–8411.
26. Balandin, A. A.; Ghosh, S.; Bao, W. Z.; Calizo, I.; Teweldebrhan, D.; Miao, F.; Lau, C. N. Superior Thermal Conductivity of Single-Layer Graphene. *Nano Lett.* **2008**, *8*, 902–907.
27. Qu, L.; Liu, Y.; Baek, J.-B.; Dai, L. Nitrogen-Doped Graphene as Efficient Metal-Free Electrocatalysts for Oxygen Reduction Reaction in Fuel Cells. *ACS Nano* **2010**, *4*, 1321–1326.
28. Li, X.; Wang, H.; Robinson, J. T.; Sanchez, H.; Diankov, G.; Dai, H. Simultaneous Nitrogen Doping and Reduction of Graphene Oxide. *J. Am. Chem. Soc.* **2009**, *131*, 15939–15944.
29. Geng, D.; Chen, Y.; Chen, Y.; Li, Y.; Li, R.; Sun, X.; Ye, S.; Knights, S. High Oxygen-Reduction Activity and Durability of Nitrogen-Doped Graphene. *Energy Environ. Sci.* **2011**, *4*, 760–764.
30. Lin, Y.-C.; Lin, C.-Y.; Chiu, P.-W. Controllable Graphene N-Doping with Ammonia Plasma. *Appl. Phys. Lett.* **2010**, *96*, 133110.

31. Wang, X. C.; Maeda, K.; Thomas, A.; Takanabe, K.; Xin, G.; Carlsson, J. M.; Domen, K.; Antonietti, M. A Metal-Free Polymeric Photocatalysts for Hydrogen Production from Water Under Visible Light. *Nat. Mater.* **2009**, *8*, 76–80.
32. Zhang, Y.; Thomas, A.; Antonietti, M.; Wang, X. Activation of Carbon Nitride Solids by Protonation: Morphology Changes, Enhances Ionic Conductivity and Photoreduction Experiments. *J. Am. Chem. Soc.* **2009**, *131*, 50–51.
33. Lee, K. R.; Lee, K. U.; Lee, J. W.; Ahn, B. T.; Woo, S. I. Electrochemical Oxygen Reduction on Nitrogen Doped Graphene Sheets in Acid Media. *Electrochem. Commun.* **2010**, *12*, 1052–1055.
34. Sheng, Z. H.; Shao, L.; Chen, J. J.; Bao, W. J.; Wang, F. B.; Xia, X. H. Catalyst-Free Synthesis of Nitrogen-Doped Graphene *via* Thermal Annealing Graphite Oxide with Melamine and Its excellent Electrocatalysis. *ACS Nano* **2011**, *5*, 4350–4358.
35. Côté, R.; Lalandc, G.; Guay, D.; Dodclct, J. P.; Dćnćs, G. Influence of Nitrogen-Containing Precursors on the Electrocatalytic Activity of Heat-Treated $Fe(OH)_2$ on Carbon Black for O_2 Reduction. *J. Electrochem. Soc.* **1998**, *145*, 2411–2418.
36. Kim, T. W.; Park, I. S.; Ryoo, R. A Synthetic Route to Ordered Mesoporous Carbon with Graphitic Pore Walls. *Angew. Chem., Int. Ed.* **2003**, *42*, 4375–4379.
37. Chen, Z.; Higgins, D.; Tao, H.; Hsu, R. S.; Chen, Z. Highly Active Nitrogen-Doped Carbon Nanotubes for Oxygen Reduction Reaction in Fuel Cell Application. *J. Phys. Chem. C* **2009**, *113*, 21008–21013.
38. Liu, G.; Li, X.; Lee, J. W.; Popov, B. N. A Review of the Development of Nitrogen-Modified Carbon-Based Catalysts for Oxygen Reduction as USC. *Catal. Sci. Technol.* **2011**, *1*, 207–217.
39. Rao, C. V.; Caberea, C. R.; Ishikawa, Y. In Search of the Active Site in Nitrogen-Doped Carbon Nanotube Electrodes for the Oxygen Reduction Reaction. *J. Phys. Chem. Lett.* **2010**, *1*, 2622–2627.
40. Jeon, I. Y.; Yu, D.; Bae, S. Y.; Choi, H. J.; Chang, D. W.; Dai, L.; Baek, J. B. Formation of Large-Area Nitrogen-Doped Graphene Film Prepared from Simple Solution Casting of Edge-Selectively Functionalized Graphite and Its Electrocatalytic Activity. *Chem. Mater.* **2011**, *23*, 3987–3992.
41. Mo, Z.; Liao, S.; Zheng, Y.; Fu, Z. Preparation of Nitrogen-Doped Carbon Nanotube Arrays and Their Catalysis towards Cathodic Oxygen Reduction in Acidic and Alkaline Media. *Carbon* **2012**, *50*, 2620.
42. Kothandaraman, R.; Nallathambi, V.; Artyushkova, K.; Barton, S. C. Non-Precious Oxygen Reduction Catalysts Prepared by High-Pressure Pyrolysis for Low-Temperature Fuel Cell. *Appl. Catal., B* **2009**, *92*, 209–216.
43. Herzog, B.; Herein, D.; Schlögl, R. *In Situ* X-ray Powder Diffraction Analysis of the Microstructure of Activated Iron Catalysts for Ammonia Synthesis. *Appl. Catal. A: Gen.* **1996**, *141*, 71–104.
44. Lafèvre, M.; Dodelet, J. P.; Bertrand, P. Molecular Oxygen Reduction in PEM Fuel Cells: Evidence for the Simultaneous Presence of Two Active Sites in Fe-Based Catalysts. *J. Phys. Chem. B* **2002**, *106*, 8705–8713.
45. Bailey, L. D.; Ttrudeau, M.; Joly, A.; Schulz, R.; Lalande, G.; Guay, D.; Dodelet, J. P. Graphitization and Particles Size Analysis of Pyrolyzed Cobalt Phthalocyanine/Carbon Catalysts for Oxygen Reduction in Fuel Cells. *J. Mater. Res.* **1994**, *9*, 3202–3209.
46. Gojković, S. L.; Gupta, S.; Savinell, R. F. Heat-Treated Iron(III) Tetramethoxyphenyl Porphyrin Chloride Supported on High-Area Carbon as an Electrcatalysts for Oxygen Reduction. *J. Electroanal. Chem.* **1999**, *462*, 63–72.
47. Subramanian, N. P.; Li, X; Nallathambi, V; Kumaraguru, S. W.; Mercado, H. C.; Wu, G.; Lee, J. W.; Popov, B. N. Nitrogen-Modified Carbon-Based Catalysts for Oxygen Reduction Reaction in Polymer Electrolyte Membrane Fuel Cells. *J. Power Sources* **2009**, *188*, 38–44.
48. Hummers, W. S.; Offeman, R. E. Preparation of Graphitic Oxide. *J. Am. Chem. Soc.* **1958**, *80*, 1339.